4-2022

Quasi In-Situ EBSD Analysis of Twinning-Detwinning and Slip Behaviors in Textured AZ31 Magnesium Alloy Subjected to Compressive-Tensile Loading

Yuzhi Zhu
Washington State University

Dewen Hou
Boise State University

Qizhen Li
Washington State University

Available online at www.sciencedirect.com

ScienceDirect

Journal of Magnesium and Alloys 10 (2022) 956–964

www.elsevier.com/locate/jma

Full Length Article

Quasi in-situ EBSD analysis of twinning-detwinning and slip behaviors in textured AZ31 magnesium alloy subjected to compressive-tensile loading

Yuzhi Zhu[a], Dewen Hou[b], Qizhen Li[a,*]

[a] School of Mechanical and Materials Engineering, Washington State University, Pullman, WA 99164, United States
[b] Micron School of Materials Science and Engineering, Boise State University, Boise 83725-1030 ID, United States

Received 21 June 2021; received in revised form 11 August 2021; accepted 18 August 2021
Available online 14 October 2021

Abstract

Twinning and detwinning behavior, together with slip behavior, are studied in a textured AZ31 magnesium alloy under compressive and tensile strains along the rolling direction (RD) after each interrupted mechanical test via quasi in-situ electron backscattered diffraction technique. The results show that twinning firstly takes place under the compressive strain along the RD. With the increasing compressive strain, $\{10\bar{1}2\}$ tensile twins firstly nucleate, then propagate, and finally thicken. While under a reversed tensile strain along the RD, detwinning occurs. No nucleation happens during detwinning. Thus, tensile twins can detwin at lower tensile strain, followed by thinning, shortening, and vanishing. Slips are also activated to accommodate the plastic deformation. In the matrix, prismatic slip can only dominate at relatively high strains. Otherwise, basal slip dominates. While in the twins, prismatic slip can activate at lower strains, which is ascribed to the texture reorientation.

Keywords: Magnesium alloy; Twinning; Detwinning; Prismatic slip; quasi in-situ EBSD.

1. Introduction

Twinning and detwinning play an important role in plastic deformation for hcp structure materials [1, 2], as hexagonal materials cannot offer enough numbers of slip systems during deformation [3–6]. The most common and easily activated twinning mode in magnesium alloys is $\{10\bar{1}2\}$ tensile twinning at room temperature [7–10]. Tensile twinning can only be activated under c-axis extension [11–13]. Consequently, it should exhibit an asymmetric deformation behavior on a textured magnesium alloy, i.e., rolled or extruded material, with a lower yield strength under compression and a higher yield strength under tension [14–17].

Generally, detwinning of the $\{10\bar{1}2\}$ tensile twins can occur under two loading conditions: (1) reloading along the opposite direction after the pre-loading; and (2) re-compression along the orthogonal direction after the pre-compression along the RD [18–22]. Therefore, twinning and detwinning usually can be observed when cyclic loadings are applied. With a limited number of fatigue cycles, the deformation was mainly dominated by twinning/detwinning mode [23, 24]. Furthermore, the fracture morphology was controlled by the repeated twinning-detwinning process [25]. The twinning/detwinning under different strain paths can lead to different mechanical responses [26, 27]. Pre-compressive deformation usually caused a drop in the tensile yield strength [28, 29]. Previous research reported that the activation of detwinning increased the work hardening rate [23, 30]. It was also found that not only twinning-slip interaction but twinning-detwinning activity could result in the Bauschinger effect, due to the stress relaxation during the detwinning process [31–33].

The main explanation of the twinning-detwinning behavior is that the process is controlled by the migration of twin boundaries (TBs) [34–36]. Compared to the twinning nucle-

* Corresponding author.
E-mail addresses: zhuyuzhi@ustb.edu.cn (Y. Zhu), dewenhou@boisestate.edu (D. Hou), qizhen.li@wsu.edu (Q. Li).

https://doi.org/10.1016/j.jma.2021.08.025

ation process, the propagation process needs much lower energy, i.e., CRSS $_{nucleation}$ > CRSS $_{propagation}$ [37]. Moreover, the process of detwinning does not need nucleation [38, 39]. As a result, detwinning can take place under a stress even lower than the CRSS for twin growth, which is attributed to the internal stress in the grain matrix generated during twinning. It was reported that CRSS values for $\{10\bar{1}2\}$ tensile twinning and detwinning in wrought ZK60A alloys are 15 MPa and 6 MPa, respectively [40].

Besides the twinning and detwinning mechanisms, there should be the activations of slips to accommodate the plastic deformation. The different activations of slips, twinning, and detwinning during the loading path change should be responsible for the asymmetric deformation behaviors [41, 42]. Several simulation results suggested that during the loading path change process, the activities of the slip systems changed both in the matrix and the twins due to the texture reorientations [43–45]. Hama et al. [44] suggested that during the reloading process under tension, there was a transfer from the detwinning-dominated mode to the slip-dominated mode as the tensile strain increased. Wang et al. [45] found increased activation of the prismatic slip system during the reversed shear loading under cyclic shear. However, there is a lack of experimental study on slip behaviors during the loading path change process.

To date, the twinning-detwinning phenomenon was observed to take place under cyclic loading or different strain paths. However, there is still a lack of study focusing on the twinning-detwinning behaviors, associated with the twinning/detwinning-slip interactions during the loading path change in rolled AZ31 magnesium alloy. The purpose of this paper is to understand the evolution of twinning/detwinning, as well as the dislocation slips, subjected to two cycles of compressive-tensile loadings along the RD in a textured AZ31 magnesium alloy sheet. The microstructure and texture evolutions were investigated by the quasi in-situ EBSD technique.

2. Experimental methods

A commercial rolled AZ31 magnesium alloy with a thickness of 20 mm was used in this study. The specimen with a dog-bone shape was cut from the as-received rolled AZ31 magnesium alloy using an electrical discharge machine, with a gage length of 8 mm (RD), a thickness of 10 mm (ND), and a width of 4 mm (TD). Here, RD, ND, and TD represent rolling direction, normal direction, and transverse direction, respectively. Mechanical tests were carried out in a CMT 5150 machine. Both tensile and compression tests were processed along the RD at room temperature with a strain rate of 10^{-3} s^{-1}. Mechanical tests were interrupted at certain deformation strains to obtain the mechanical responses and evaluate the microstructure evolution of the AZ31 magnesium specimen.

Electron back-scattered diffraction (EBSD) measurements were performed in a JOEL-JEM 7800F field emission scanning electron microscope (SEM) equipped with Aztec and HKL Channel 5 software. The scanning step size is 0.7 μm.

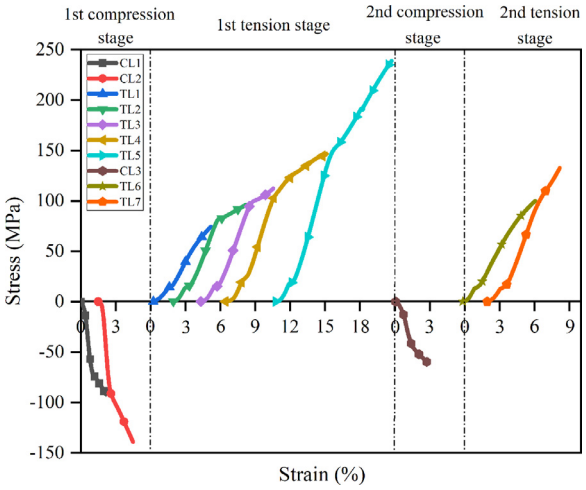

Fig. 1. Compressive and tensile stress-strain curves along the RD to different strain levels.

The deformed specimen for EBSD measurement was mechanically polished, followed by electrochemical polishing with AC2 solutions. EBSD measurements were carried out in the sample at a certain region parallel to the RD-TD plane after each deform stage.

3. Results and discussion

3.1. Mechanical behaviors

The successive deformation stress-strain curves are exhibited in Fig. 1, including compression and tension along the RD to different strain levels. The stress-strain curve above the x-axis in the diagram represents the tensile test, and the curve below the x-axis represents the compression test. The sample initially deformed under two successive compression tests (denoted as CL1 and CL2) with a pre-strain of 1.3% and 3.2%, respectively, in the first compression stage. It is observed that the compressive stress-strain curve contains a yield plateau, which indicates the tensile twinning activation during the compression test with the deformation load perpendicular to the c-axis [46, 47]. In the first tension stage, the pre-strained sample was then deformed under tensile loading to strains of 1.6%, 4.8%, 7.6%, 11%, and 14.6%, respectively. The tensile stress-strain curves (denoted as TL1, TL2, TL3, TL4, and TL5, respectively) show similar deformation behaviors that all exhibit a typical convex shape. An increment of the yield strength after each tensile deformation can be observed. This increment can result from the strain hardening effect during the deformation, where tangled dislocations prevent further dislocation movements [48]. After then, at the second compression stage, a compressive deformation with a strain of 0.9%, was conducted. A similar stress-strain curve (denoted as CL3) is plotted as those in the first compression stage, indicating the similar deformation mode activations in this deformation stage. Finally, in the second tension stage, two steps of the successive tension deformations (de-

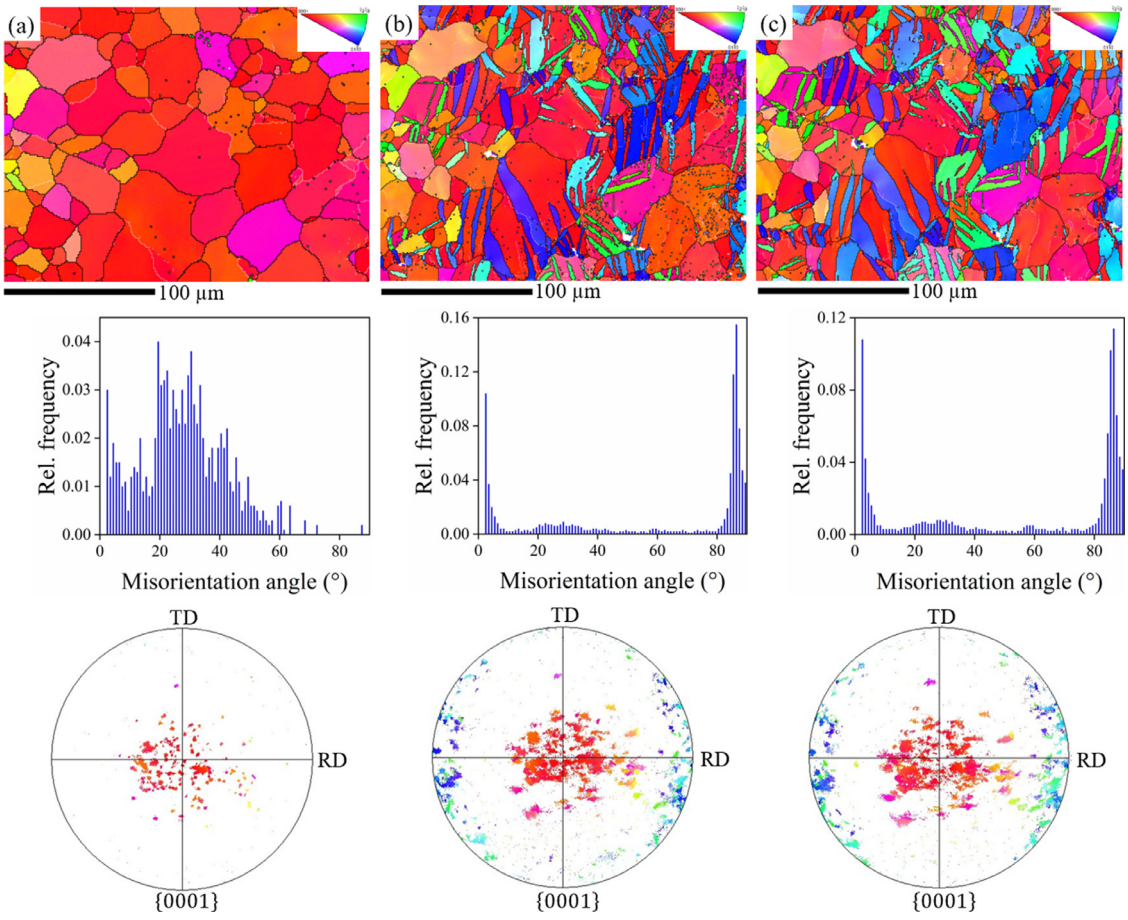

Fig. 2. EBSD inverse pole figure (IPF) maps, misorientation angle distributions, and {0001} pole figures for the rolled AZ31 magnesium alloy sample: (a) the initial state; (b) pre-compressed to 1.3% along the RD; (c) pre-compressed to 3.2% along the RD.

noted as TL6 and TL7, respectively) were carried out. The tensile strains can be clarified as 1.6% and 4%, respectively.

3.2. Microstructure evaluation after each deform stage

Figure 2 presents the IPF maps, the misorientation angle profiles, and the {0001} pole figures to illustrate the initial-state microstructure and the microstructure evolutions of the sample compressed to the pre-strain of 1.3% (CL1) and 3.2% (CL2), respectively. Figure 2a shows the initial microstructure and texture of the textured AZ31 magnesium alloy. The sample exhibits an equiaxed grain structure with the grain size ranging from ~5 to ~50 μm in the IPF map. No twins are detected in the initial microstructure. The boundary misorientation angle distribution ranges from 10 to 60°, which indicates that the predominant boundaries in the initial-state sample are high angle grain boundaries (HAGBs). In this work, HAGBs are defined as grain boundaries with a misorientation angle greater than 15° and low angle grain boundaries (LAGBs) contain a misorientation angle from 2 to 15° The {0001} pole figure in Fig. 2a reveals that the initial state sample has a typical basal texture that the c-axis of the unit cell is parallel to the ND. Figure 2b shows the microstructure of the sample at 1.3% pre-compressive strain along the RD. Many twins newly appeared in the matrix grains as can be seen in the IPF map. After CL1, two peaks, ranging from 2 to 15° and 80–90°, generate in the misorientation angle distribution histogram. The peaks ranging from 2 to 15° result from the generation of the LAGBs during compression. While the peaks ranging from 80 to 90° are attributed to the activation of the twin lamellae, which is consistent with the result in the IPF map in Fig. 2b. Furthermore, it indicates that the active twins are of $\{10\bar{1}2\}$ type, as the misorientation angle tilts ~86.3°. It is known that $\{10\bar{1}2\}$ tensile twins are easily activated under compressive strain perpendicular to or under tensile strain parallel to the c-axis of the HCP lattice [49]. An increase of the twinning component and a decrease of the basal component can be observed from the {0001} pole figure in Fig. 2b. Figure 2c shows the microstructure of the sample at 3.2% compression strain. Twinning took place in nearly all matrix grains with a soft orientation. The existing $\{10\bar{1}2\}$ tensile twins continued propagating, thickening, and further coalesced at the CL2 stage, leading to the disappearance of some twin boundaries. Thus, the peaks of the grain boundary misorientation angle ranging from 80 to 90°, as can be seen, decrease slightly due to the coalescence of the existing twin lamellae. While the texture changed little under CL2, as shown in the pole figure in Fig. 2b.

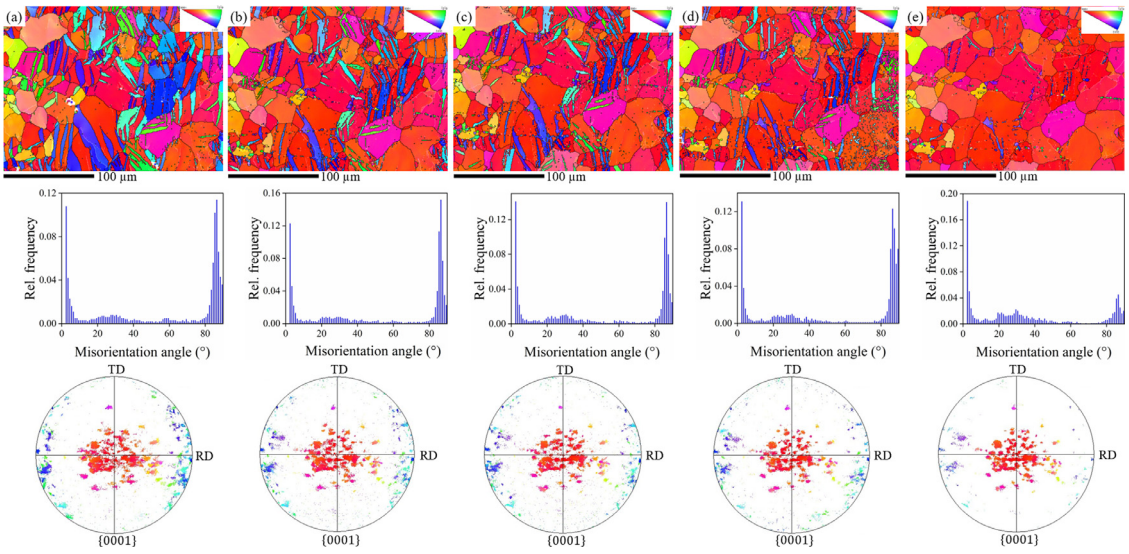

Fig. 3. EBSD inverse pole figure (IPF) maps, misorientation angle distributions, and {0001} pole figures of the AZ31 magnesium alloy under reversed tension loading: (a) reversely tension to 1.6%; (b) reversely tension to 4.8%; (c) reversely tension to 7.6%; (d) reversely tension to 11%; (e) reversely tension to 14.6%.

Figure 3 exhibits the IPF maps, the misorientation angle distributions, and the {0001} pole figures for the pre-strained sample deformed after successive reversed tensile loadings along the RD. The detwinning phenomenon is observed during the deformation process. In Fig. 3a, when a 1.6% tensile strain (TL1) was applied to the pre-compressed sample, no significant change in the microstructure can be observed. Moreover, when the applied strain increased to 4.8% (TL2), nearly all $\{10\bar{1}2\}$ tensile twins became thinner, as seen in the IPF map in Fig. 3b. Additionally, some extremely thin twin lamellae disappeared. In the misorientation angle distribution profile, the peaks ranging from 80 to 90° increase, since the coalesced twins started to disperse, and new twin boundaries were generated. As can be observed in the {0001} pole figure (Fig. 3b) for the sample at TL2, the basal pole also tilts slightly back to the ND. In Fig. 3c and d, as the tensile strain increased from 7.6% (TL3) to 11% (TL4), twin lamellae continued to become thinner and shorter. Finally, only several twin lamellae vanished. The distributions of the grain boundary misorientation angle and the textures after TL3 and TL4 do not change too much. In Fig. 3e, when the reversed tensile strain was up to 14.6% (TL5), nearly all the $\{10\bar{1}2\}$ tensile twins vanished, but only several extremely thin twin lamellae remained. The remaining thin twin lamellae may result from the incomplete reversed tensile deformation. From the grain boundary misorientation angle histogram, the peaks ranging from 80 to 90° decrease drastically, consistent with the microstructure observation that almost fully detwinning occurred in all matrix grains. While the peaks ranging from 2 to 15° increase. It is suggested that twin boundaries are replaced by LAGBs during detwinning [50]. As seen from the {0001} pole figure in Fig. 3e, the basal pole tilts back to the ND. More specifically, the reversed tensile loading along RD renders c-axis re-aligning perpendicular to the ND, while the pre-formed tensile twins from compression disappear. As reported in the previous study, the mechanism of detwinning can be considered as the reversed process of twinning [35, 51]. It is known that the twinning propagation is controlled by the movement of TBs [52]. TBs consist of coherent twin boundaries (CTBs), basal-prismatic (BPs), and prismatic-basal (PBs) facets. The evolution of twinning/detwinning then can be considered as the glide or climb of twinning dislocations along these interfaces, resulting in the migration of TBs. Consequently, the residual twins become thinner and shorter.

Figure 4 shows the IPF maps, the distribution of misorientation angle, and the {0001} pole figures for the sample under a repeated process of compression and tension. In Fig. 4a, under re-compression with a 0.9% strain (CL3), a limited number of thin twin lamellae nucleated. While there is no significant growth of the existing tensile twins. In the misorientation angle distribution histogram, the consistent results can be observed that the peaks ranging from 80 to 90° increase slightly. It is also found that re-twinning at the CL3 stage takes place at the same locations as that in the pre-compression stage. A similar phenomenon of the second-generation twin was observed in pure Mg under cyclic loading via in-situ TEM [53]. It might be explained that twinning prefers to nucleate at specific sites. Figure 5b shows the detwinning phenomenon under the reversed 1.6% tensile strain (TL6). Due to the limited tensile strain, only several thin twins became narrower. No significant change can be observed neither from the grain boundary misorientation angle distribution nor from the {0001} pole figure. As the tensile strain increased to 4% (TL7), most of the residual twin lamellae vanished, as can be observed from the IPF map in Fig. 4c. At the same time, in the misorientation angle distribution histogram, the peaks ranging from 80 to 90° decrease to nearly zero, while the fraction of the LAGBs increase. The {0001} pole figure shows a basal texture with only a small fraction of the c-axis distributed away from the ND.

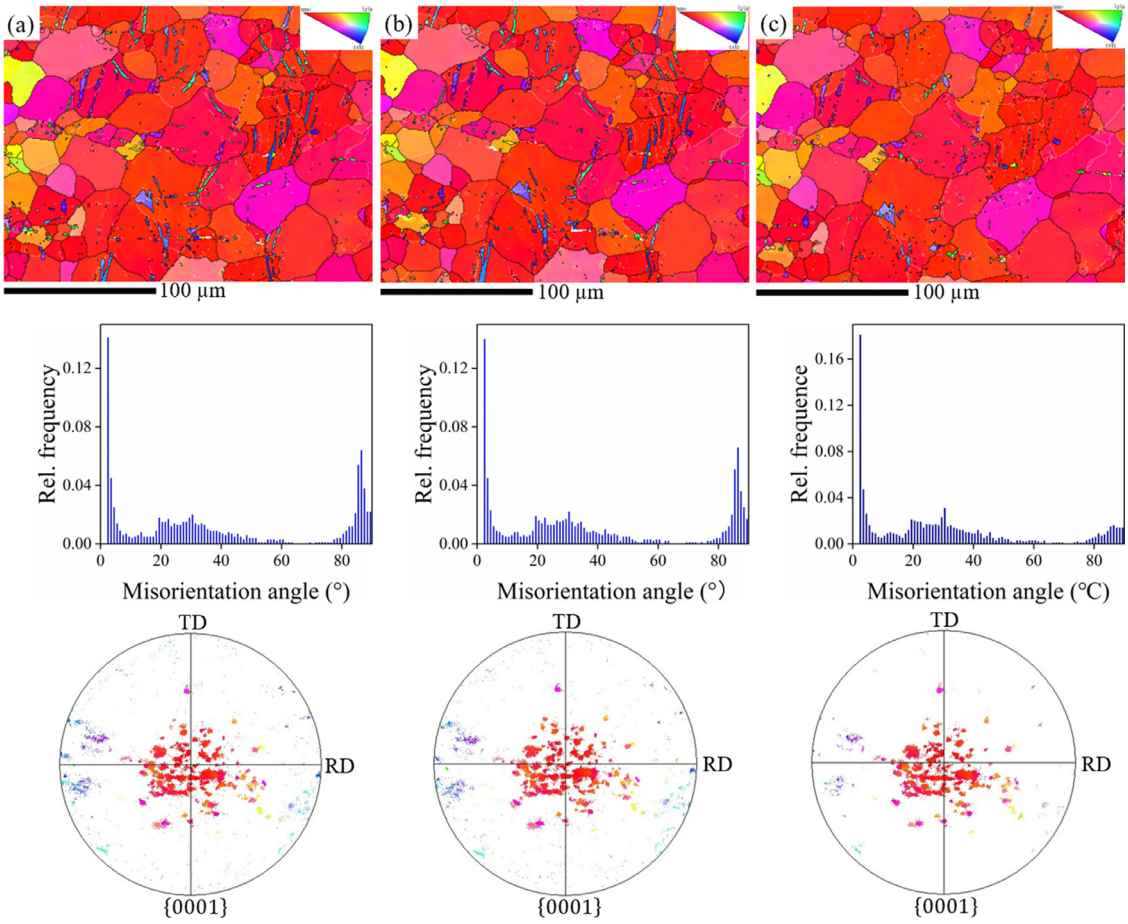

Fig. 4. EBSD inverse pole figure (IPF) maps, misorientation angle distributions, and {0001} pole figures of the AZ31 magnesium alloy under repeated compression and tension loading: (a) compression to 0.9%; (b) reversely tension to 1.6%; (c) reversely tension to 4%.

To study the interactions between twining and slip, the in-grain misorientation axis (IGMA) analysis, associated with the Schmid factor (SF) analysis was applied. Theoretically, the activation of slips can cause lattice rotations, which in term can be detected by electron backscattered diffraction. The detailed in-grain misorientation axis distribution method is introduced by Chun et al. [54, 55]. For each slip system in magnesium, they tilt around a certain axis (also named as Taylor axis). Namely, the $\{0002\}\langle 11\bar{2}0\rangle$ basal slip, the $\{10\bar{1}0\}\langle 11\bar{2}0\rangle$ prismatic slip, and the $\{11\bar{2}2\}\langle 11\bar{2}\bar{3}\rangle$ pyramidal slip have the $\langle 0\bar{1}10\rangle$, $\langle 0001\rangle$, and $\langle 1\bar{1}00\rangle$ Taylor axis, respectively. Therefore, the identifications of the slip types both in the matrix and the twins can be studied via the IGMA method. The IGMA distributions during the twinning and de-twinning process in four selected twinned/untwined grains are calculated. The misorientation angle concerned in this work is from 0.5° to 2°. And to obtain accurate results, only matrix and twins with more than 400 measured points are chosen. Figure 5 shows the IGMA distribution of four selected grains in rolled AZ31 magnesium alloy under repeated compression and tension loadings along the RD. The selected matrix grains and twins are marked as M1∼M4 and T2∼T4, respectively. The loading condition and the maximum/minimum intensity are given at the top-left corner of each figure. Table 1 shows the SF calculations for grains illustrated in Fig. 5.

Figure 5a shows the IGMA distributions in an untwined grain (marked as M1). The IGMA distributions are mainly concentrated around ⟨uvt0⟩ directions. As mentioned above, the <uvt0>-type rotation results from the activation of ⟨a⟩ type basal and $\langle c+a\rangle$ type pyramidal slips. Considering the high CRSS for <c+a> type pyramidal slip and the relatively low Schmid factor (SF) values shown in Table 1, the activation of $\langle c+a\rangle$ type dislocations is difficult. It can be assumed that in M1 during the repeated compression and tension loadings, the dominant slip mode is always the ⟨a⟩ type basal slip. Figure 5b exhibits the IGMA distributions in a twinned grain, where the matrix is marked as M2, and the twin is marked as T2. Similarly, during the pre-compression process (CL1 and CL2), the axis distributions in the matrix M2 are concentrated around ⟨uvt0⟩ directions. Under the reversed tension along the RD, from TL1 to TL4, the IGMA distribution is focused around the ⟨uvt0⟩ axis. As the tensile strain increased to 14.6% (shown in TL5) during the detwinning process, the maximum intensity of the IGMA in the matrix rotates around the ⟨0001⟩ axis. It is proposed that ⟨a⟩ type prismatic slips are more favorable at the TL5 stage. Consistently, the SF value

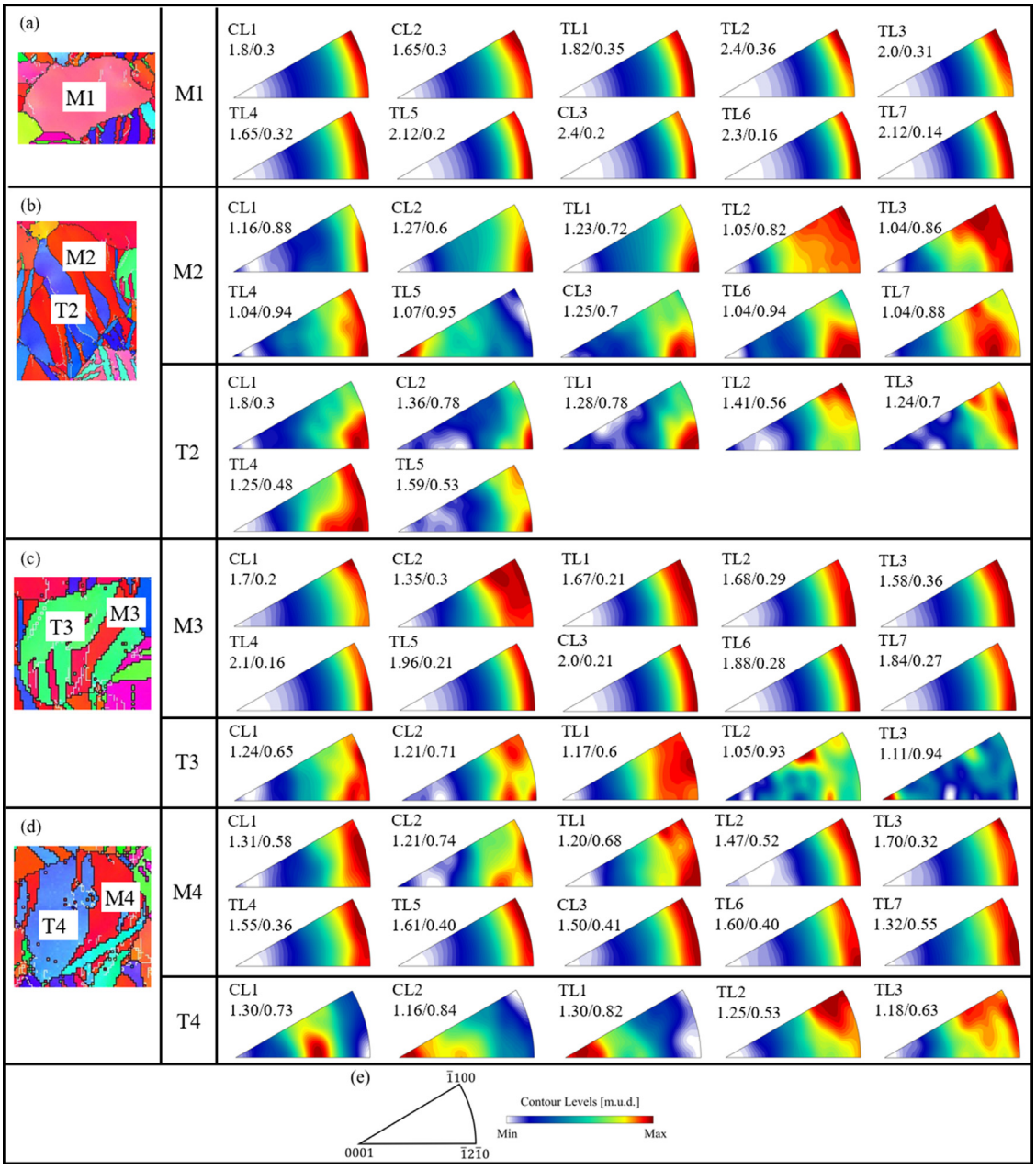

Fig. 5. The in-grain misorientation axis (IGMA) distributions of selected grains in AZ31 magnesium alloy under repeated compression and tension loadings. The maximum/minimum intensities of the IGMA distributions are given at the top of each figure.

Table 1
Schmid factors for grains illustrated in Fig. 5.

NO.	RD-Compression			RD-Tension		
	$<a>$ basal	$<a>$ prismatic	$<c+a>$ pyramidal	$<a>$ basal	$<a>$ prismatic	$<c+a>$ pyramidal
M1	0.461	0.268	0.226	0.461	0.268	0.22
M2	0.224	0.453	0.035	0.224	0.453	0.43
T2	0.338	0.063	0.48	0.338	0.063	−0.176
M3	0.217	0.467	0.007	0.217	0.307	0.486
T3	0.164	0.485	0	0.164	0.485	0.471
M4	0.287	0.451	0.051	0.287	0.451	0.463
T4	0.228	0.464	0.033	0.228	0.464	0.448

for prismatic slip in M2 is the highest, which means prismatic slip should be easily activated when the applied stress is high enough. Next, under the repeated relatively low compressive and tensile strains, the maximum intensities are around the ⟨uvt0⟩ axis. The slip behaviors in the twin T2 are different from that in the matrix M2. During the whole loading process, including the twinning and the detwinning process, the lattice rotation distributions are concentrated around the ⟨uvt0⟩ axis, indicating either ⟨a⟩ type basal or ⟨$c + a$⟩ type pyramidal slip dominates. According to the SF calculations in Table 1, during the twinning process, ⟨$c + a$⟩ type pyramidal slip possesses the highest SF value, while during the detwinning process, ⟨a⟩ type basal slip is more favorable. In Fig. 5c, the IGMA distributions in the matrix M3 and the twin T3 are presented. In M3, the maximum intensities of the IGMA are mostly around the ⟨uvt0⟩ axis, which suggests that during the whole process, ⟨a⟩ type basal and ⟨$c + a$⟩ type pyramidal slips are favorable. At the CL2 stage, the IGMA distribution spread out towards the ⟨0001⟩ direction, indicating the activation of ⟨a⟩ type prismatic slip, which is consistent with the SF calculation shown in Table 1. During the twinning process, the IGMA distributions in the twin T3 are concentrated in the ⟨uvt0⟩ direction. Considering the lowest CRSS and the second highest SF value (in Table 1), it is reasonable to say ⟨a⟩ type basal slips are dominant in T3. While during the detwinning process, as the tensile strain increased to 7.5%, the IGMA distribution concentrations tilt from the ⟨uvt0⟩ direction to the ⟨0001⟩ direction. And the SF value for prismatic slip is the highest. Therefore, ⟨a⟩ type prismatic slips are activated. The twinning/detwinning operation, which re-orientates the grains with a hard orientation for slip, contributes to the prismatic slip activation. Figure 5d shows the IGMA distributions in the matrix M4 and the twin T4. Similarly, the maximum intensities of M4 are around the ⟨uvt0⟩ axis during the whole deformation process. According to the SF results, both ⟨a⟩ type basal and ⟨$c + a$⟩ type pyramidal slips are favorable. The IGMA distribution in T4 at 1.3% pre-compressive strain is concentrated around the ⟨uvt0⟩ direction. While as the pre-strain increased to 3.2%, the IGMA distribution rotates to the ⟨0001⟩ direction, suggesting that the ⟨a⟩ type prismatic slips dominate at this stage. At the TL1 stage (ε=1.6%), prismatic slip is still preferred in T4. While as the reversed tensile strain increased to 4.8% and higher, the IGMA distribution concertation transfers to the ⟨uvt0⟩ direction. Because at these stages, the twin T4 vanishes very quickly, we assume the twin size can also affect the slip activations [56].

4. Conclusions

In this work, the quasi in-situ electron backscattered diffraction technique was used to study the twinning and detwinning behaviors on a rolled AZ31 magnesium alloys under compression and tension along the RD after interrupted mechanical tests. The slip behavior analysis was conducted by the in-grain misorientation axis distribution method and Schmid factor method. Pre-compression tests revealed that $\{10\bar{1}2\}$ tensile twins nucleated at low compressive strains, then further propagated and thickened with increasing strains. The microstructure evolution during reversed tensile tests along the RD exhibited the detwinning process. At a relatively low reversed tensile strain, the existing tensile twins started to become thinner. With the increasing reversed strain, twins continued thinning, shortening, and finally vanishing. Under repeated compressive and tensile loadings along the RD, re-twinning and re-detwinning occurred. It was also observed that re-twinning preferred to take place at the same location as in the first deformation stage. The IGMA analysis showed that the slip behaviors in the matrix and the twins were different. In the matrix, at low stains, ⟨a⟩ type basal slip was favorable. As the stain increase, it was hard to find ⟨a⟩ type prismatic slips that could dominate in the matrix. In the twins, since the texture reorientation took place, prismatic slips could be activated more easily, even at relatively low strains.

Declaration of Competing Interest

None.

Acknowledgment

The authors gratefully acknowledge the financial support from the US Department of Energy, Office of Basic Energy Science under Award no. DE-SC0016333.

References

[1] S. You, Y. Huang, K.U. Kainer, N. Hort, Recent research and developments on wrought magnesium alloys, J Magnes Alloy 5 (2017) 239–253.
[2] B. Song, N. Guo, T. Liu, Q.S. Yang, Improvement of formability and mechanical properties of magnesium alloys via pre-twinning: a review, Mater Des 62 (2014) 352–360.
[3] J. Koike, R. Ohyama, Geometrical criterion for the activation of prismatic slip in AZ61 Mg alloy sheets deformed at room temperature, Acta Mater 53 (2005) 1963–1972.
[4] S. Sandlöbes, S. Zaefferer, I. Schestakow, S. Yi, R. Gonzalez-Martinez, On the role of non-basal deformation mechanisms for the ductility of Mg and Mg–Y alloys, Acta Mater 59 (2011) 429–439.
[5] S.R. Agnew, D.W. Brown, C.N. Tomé, Validating a polycrystal model for the elastoplastic response of magnesium alloy AZ31 using in situ neutron diffraction, Acta Mater 54 (2006) 4841–4852.
[6] D. Hou, T. Liu, M. Shi, H. Wen, H. Zhao, Deformation Mechanisms in a Rolled Magnesium Alloy Under Tension Along the Rolling Direction, Micros Microanal 24 (2018) 207–213.
[7] L. Jiang, J.J. Jonas, R.K. Mishra, A.A. Luo, A.K. Sachdev, S. Godet, Twinning and texture development in two Mg alloys subjected to loading along three different strain paths, Acta Mater 55 (2007) 3899–3910.
[8] K.E. Prasad, K. Rajesh, U. Ramamurty, Micropillar and macropillar compression response of magnesium single crystals oriented for single slip or extension twinning, Acta Mater 65 (2014) 316–325.
[9] I. Enrique, N. Galindo, Modelling twinning evolution during plastic deformation in hexagonal close-packed metals, Mater Des 83 (2015) 327–343.
[10] Q. Li, Mechanical properties and microscopic deformation mechanism of polycrystalline magnesium under high-strain-rate compressive loadings, Materials Science and Engineering A (2012) 130–134.
[11] M.R. Barnett, A. Ghaderi, J.Q. Da Fonseca, J.D. Robson, Influence of orientation on twin nucleation and growth at low strains in a magnesium alloy, Acta Mater 80 (2014) 380–391.

[12] D. Hou, T. Liu, H. Chen, D. Shi, C. Ran, F. Pan, Analysis of the microstructure and deformation mechanisms by compression along normal direction in a rolled AZ31 magnesium alloy, Mater Sci Eng A 660 (2016) 102–107.
[13] S.G. Hong, S.H. Park, C.S. Lee, Role of 1012 twinning characteristics in the deformation behavior of a polycrystalline magnesium alloy, Acta Mater 58 (2010) 5873–5885.
[14] B. Song, R. Xin, G. Chen, X. Zhang, Q. Liu, Improving tensile and compressive properties of magnesium alloy plates by pre-cold rolling, Scripta Mater 66 (2012) 1061–1064.
[15] S. Pan, Y. Xin, G. Huang, Q. Li, F. Guo, Q. Liu, Tailoring the texture and mechanical anisotropy of a Mg–2Zn–2Gd plate by varying the rolling path, Mater Sci Eng A 653 (2016) 93–98.
[16] S. Pan, X. Huang, Y. Xin, G. Huang, Q. Li, C. Tan, Q. Liu, The effect of hot rolling regime on texture and mechanical properties of an as-cast Mg–2Zn–2Gd plate, Mater Sci Eng A 731 (2018) 288–295.
[17] M. Knezevic, A. Levinson, R. Harris, R.K. Mishra, R.D. Doherty, S.R. Kalidindi, Deformation twinning in AZ31: influence on strain hardening and texture evolution, Acta Mater 58 (2010) 6230–6242.
[18] L. Wang, G. Huang, Q. Quan, P. Bassani, E. Mostaed, M. Vedani, F. Pan, The effect of twinning and detwinning on the mechanical property of AZ31 extruded magnesium alloy during strain-path changes, Mater Des 63 (2014) 177–184.
[19] M. Zecevic, M. Knezevic, I.J. Beyerlein, C.N. Tomé, An elasto-plastic self-consistent model with hardening based on dislocation density, twinning and de-twinning: application to strain path changes in HCP metals, Mater Sci Eng A 638 (2015) 262–274.
[20] W. Wu, S.Y. Lee, A.M. Paradowska, Y. Gao, P.K. Liaw, Twinning–detwinning behavior during fatigue-crack propagation in a wrought magnesium alloy AZ31B, Mater Sci Eng A 556 (2012) 278–286.
[21] B.L. Wu, G.S. Duan, X.H. Du, L.H. Song, Y.D. Zhang, M.J. Philippe, C. Esling, In situ investigation of extension twinning-detwinning and its effect on the mechanical behavior of AZ31B magnesium alloy, Mater Des 132 (2017) 57–65.
[22] Q. Li, Q. Yu, J. Zhang, Y. Jiang, Effect of strain amplitude on tension–compression fatigue behavior of extruded Mg6Al1ZnA magnesium alloy, Scripta Mater 62 (2010) 778–781.
[23] T. Hama, Y. Kariyazaki, N. Hosokawa, H. Fujimoto, H. Takuda, Work-hardening behaviors of magnesium alloy sheet during in-plane cyclic loading, Mater Sci Eng A 551 (2012) 209–217.
[24] Q. Li, Q. Yu, J. Zhang, Y. Jiang, Microstructure and deformation mechanism of Mg6Al1ZnA alloy experienced tensioncompression cyclic loading, Scripta Materialia 64 (2011) 233–236.
[25] F. Briffod, T. Shiraiwa, M. Enoki, Numerical investigation of the influence of twinning/detwinning on fatigue crack initiation in AZ31 magnesium alloy, Mater Sci Eng A 753 (2019) 79–90.
[26] Y. Xin, X. Zhou, H. Chen, J.F. Nie, H. Zhang, Y. Zhang, Q. Liu, Annealing hardening in detwinning deformation of Mg–3Al–1Zn alloy, Mater Sci Eng A 594 (2014) 287–291.
[27] S. Wang, Y. Zhang, C. Schuman, J.S. Lecomte, X. Zhao, L. Zuo, M.J. Philippe, C. Esling, Study of twinning/detwinning behaviors of Ti by interrupted in situ tensile tests, Acta Mater 82 (2015) 424–436.
[28] Y.N. Wang, J.C. Huang, The role of twinning and untwinning in yielding behavior in hot-extruded Mg–Al–Zn alloy, Acta Mater 55 (2007) 897–905.
[29] H. Liu, R. Yin, Q. Zou, J. Zhang, Z. Liu, X. Zhang, Effects of micro-twin lamellar structure on the mechanical properties and fracture morphology of AZ31 Mg alloy, Mater Sci Eng A 745 (2019) 221–230.
[30] N. Yi, T. Hama, A. Kobuki, H. Fujimoto, H. Takuda, Anisotropic deformation behavior under various strain paths in commercially pure titanium grade 1 and grade 2 sheets, Materials Science and Engineering A 655 (2016) 70–85.
[31] L. Wu, A. Jain, D.W. Brown, G.M. Stoica, S.R. Agnew, B. Clausen, D.E. Fielden, P.K. Liaw, Twinning–detwinning behavior during the strain-controlled low-cycle fatigue testing of a wrought magnesium alloy, ZK60A, Acta Mater 56 (2008) 688–695.
[32] Y. Xiong, Q. Yu, Y. Jiang, An experimental study of cyclic plastic deformation of extruded ZK60 magnesium alloy under uniaxial loading at room temperature, Int J Plasticity 53 (2014) 107–124.
[33] L. Song, B. Wu, L. Zhang, X. Du, Y. Wang, C. Esling, M.J. Philippe, Detwinning-related Bauschinger effect of an extruded magnesium alloy AZ31B, Mater Charact 148 (2019) 63–70.
[34] P.D. Wu, X.Q. Guo, H. Qiao, D.J. Lloyd, A constitutive model of twin nucleation, propagation and growth in magnesium crystals, Mater Sci Eng A 625 (2015) 140–145.
[35] D. Hou, Q. Li, H. Wen, Study of reversible motion of 1012 tensile twin boundaries in a magnesium alloy during strain path changes, Mater Lett 231 (2018) 84–86.
[36] S.H. Park, J.H. Lee, Y.H. Huh, S.G. Hong, Enhancing the effect of texture control using 1012 twins by retarding detwinning activity in rolled Mg–3Al–1Zn alloy, Scripta Mater 69 (2013) 797–800.
[37] H. El Kadiri, J. Kapil, A.L. Oppedal, L.G. Hector Jr, S.R. Agnew, M. Cherkaoui, S.C. Vogel, The effect of twin–twin interactions on the nucleation and propagation of 1012 twinning in magnesium, Acta Mater 61 (2013) 3549–3563.
[38] H. Wang, P.D. Wu, J. Wang, C.N. Tomé, A crystal plasticity model for hexagonal close packed (HCP) crystals including twinning and de-twinning mechanisms, Int J Plasticity 49 (2013) 36–52.
[39] H. Qiao, S.R. Agnew, P.D. Wu, Modeling twinning and detwinning behavior of Mg alloy ZK60A during monotonic and cyclic loading, Int J Plasticity 65 (2015) 61–84.
[40] L. Wu, S.R. Agnew, D.W. Brown, G.M. Stoica, B. Clausen, A. Jain, D.E. Fielden, P.K. Liaw, Internal stress relaxation and load redistribution during the twinning–detwinning-dominated cyclic deformation of a wrought magnesium alloy, ZK60A, Acta Mater 56 (2008) 3699–3707.
[41] S.G. Hong, S.H. Park, C.S. Lee, Enhancing the fatigue property of rolled AZ31 magnesium alloy by controlling 1012 twinning-detwinning characteristics, J Mater Res 25 (2010) 784–792.
[42] A. Vinogradov, D. Orlov, A. Danyuk, Y. Estrin, Deformation mechanisms underlying tension–compression asymmetry in magnesium alloy ZK60 revealed by acoustic emission monitoring, Mater Sci Eng A 621 (2015) 243–251.
[43] G. Proust, C.N. Tomé, A. Jain, S.R. Agnew, Modeling the effect of twinning and detwinning during strain-path changes of magnesium alloy AZ31, Int J Plasticity 25 (2009) 861–880.
[44] T. Hama, N. Kitamura, H. Takuda, Effect of twinning and detwinning on inelastic behavior during unloading in a magnesium alloy sheet, Mater Sci Eng A 583 (2013) 232–241.
[45] H. Wang, P.D. Wu, J. Wang, Modelling the role of slips and twins in magnesium alloys under cyclic shear, Comp Mater Sci 96 (2015) 214–218.
[46] S.H. Choi, E.J. Shin, B.S. Seong, Simulation of deformation twins and deformation texture in an AZ31 Mg alloy under uniaxial compression, Acta Mater 55 (2007) 4181–4192.
[47] M.R. Barnett, Z. Keshavarz, X. Ma, A semianalytical Sachs model for the flow stress of a magnesium alloy, Metall Mater Trans A 37 (2006) 2283–2293.
[48] D. Sarker, D.L. Chen, Detwinning and strain hardening of an extruded magnesium alloy during compression, Scripta Mater 67 (2012) 165–168.
[49] R. Sánchez-Martín, M.T. Pérez-Prado, J. Segurado, J.M. Molina-Aldareguia, Effect of indentation size on the nucleation and propagation of tensile twinning in pure magnesium, Acta Mater 93 (2015) 114–128.
[50] Y. Cui, Y. Li, Z. Wang, X. Ding, Y. Koizumi, H. Bian, L. Lin, A. Chiba, Impact of solute elements on detwinning in magnesium and its alloys, Int J Plasticity 91 (2017) 134–159.
[51] J. Wang, L. Liu, C.N. Tomé, S.X. Mao, S.K. Gong, Twinning and de-twinning via glide and climb of twinning dislocations along serrated coherent twin boundaries in hexagonal-close-packed metals, Mater Res Lett 1 (2013) 81–88.
[52] A. Ostapovets, R. Gröger, Twinning disconnections and basal–prismatic twin boundary in magnesium, Model Simul Mater Sci Eng 22 (2014) 025015.
[53] B.M. Morrow, R.J. McCabe, E.K. Cerreta, C.N. Tomé, In-situ TEM observation of twinning and detwinning during cyclic loading in Mg, Metall Mater Trans A 45 (2014) 36–40.

[54] Y.B. Chun, M. Battaini, C.H.J. Davies, S.K. Hwang, Distribution characteristics of in-grain misorientation axes in cold-rolled commercially pure titanium and their correlation with active slip modes, Metall Mater Trans A 41 (2010) 3473–3487.
[55] Y.B. Chun, C.H.J. Davies, Investigation of prism < a>slip in warm-rolled AZ31 alloy, Metall Mater Trans A 42 (2011) 4113–4125.
[56] C.M. Cepeda-Jiménez, J.M. Molina-Aldareguia, M.T. Pérez-Prado, Effect of grain size on slip activity in pure magnesium polycrystals, Acta Mater 84 (2015) 443–456.